Progress in Nuclear Energy 110 (2019) 213–223

Contents lists available at ScienceDirect

Progress in Nuclear Energy

journal homepage: www.elsevier.com/locate/pnucene

Numerical approach to study the thermal-hydraulic characteristics of Reactor Vessel Cooling system in sodium-cooled fast reactors

Ping Song[a], Dalin Zhang[a,*], Tangtao Feng[a], Shibao Wang[a], Jing Chen[a], Xin'an Wang[a], Xiuli Xue[b], Yapei Zhang[a], Mingjun Wang[a], Suizheng Qiu[a], G.H. Su[a]

[a] School of Nuclear Science and Technology, State Key Laboratory of Multiphase Flow in Power Engineering, Xi'an Jiaotong University, No. 28, Xianning West Road, Xi'an, 710049, China
[b] China Institute of Atomic Energy, China

ARTICLE INFO

Keywords:
Reactor vessel cooling system
Code development
Sodium-cooled fast reactor
Sensitivity analysis

ABSTRACT

The main vessel plays an important role in containing the entire primary sodium for pool-type sodium-cooled fast reactors (SFRs). The Reactor Vessel Cooling System (RVCS) has great effect on cooling the main vessel. However, little attention has been given to the study on transient characteristics of RVCS in the previous SFR research. Thus, a home-made one-dimensional (1-D) code named Reactor Vessel Cooling system Analysis Code for Sodium-cooled fast reactor (VECAS) is proposed to evaluate the thermal-hydraulic characteristics for SFR. The detailed models of the developed VECAS are presented in this paper. Moreover, the developed models have been validated against an experimental study. Numerical data of the main vessel cooling circuit are compared with the measurements of the Demonstration Fast Breeder Reactor (DFBR). The simulation results are in good agreement with the experimental data. Furthermore, the validated VECAS is coupled with the Transient Thermal-Hydraulic Analysis Code for Sodium-cooled fast reactors (THACS). The transient characteristics of RVCS in China Experimental sodium-cooled Fast Reactor (CEFR) are simulated by the coupled code. Steady analysis shows that the main vessel is cooled effectively. The peak temperature appears at the top of the main vessel lower than the permissible upper temperature limit. During the transient analysis, VECAS has predicted a reverse flow in RVCS, which contributes to the core cooling. Furthermore, sensitivity analysis of the main parameter has also been performed. Therefore, it can be concluded that coupled VECAS has the ability to evaluate the thermal-hydraulic characteristics as well as the decay heat removal capacity of RVCS. The coupled code could provide references and technical supports for the design and optimization of the pool-type sodium-cooled fast reactor.

1. Introduction

CHINA is enhancing the development of generation IV advanced nuclear power systems (Zhang et al., 2018). As one of the 6 candidate Generation-IV reactors (Chen et al., 2018), Sodium-cooled Fast Reactor (SFR) is more effective in using uranium resources and transmuting long-life high level radioactive waste, which contributes to the sustainable development of nuclear fission energy (Ma et al., 2015). Thus, more and more importance is attached to SFRs by countries all over the word.

Fig. 1 presents the reactor structure of Indian Prototype Fast Breeder Reactor (PFBR), which is a typical pool-type sodium-cooled reactor (Velusamy et al., 2010). Fig. 2 shows another typical pool-type SFR China Experimental sodium-cooled Fast Reactor (CEFR). As shown in Figs. 1 and 2, the entire primary sodium is contained in the main vessel, which is a critical component for pool-type sodium-cooled reactors. The main vessel is very close to the hot sodium inevitably. The core outlet temperature of PFBR reaches up to 547 °C (Chetal et al., 2006). The sodium temperature in the hot pool is very high for the reason that the sodium heated in the core flows into the hot pool directly. The main vessel made of stainless steel will exceed its limiting temperature value easily. Therefore, it's of great necessity to cool the main vessel by cold liquid sodium.

The Reactor main Vessel Cooling System (RVCS) is designed to cool the main vessel and enhance its structural integrity. The schematic drawing of a typical RVCS is shown in Fig. 3. Generally, two concentric baffles are installed in the inner side of the main vessel, named inner thermal vessel and outer thermal baffle. What's more, inner vessel is

* Corresponding author.
E-mail address: dlzhang@mail.xjtu.edu.cn (D. Zhang).

https://doi.org/10.1016/j.pnucene.2018.09.021
Received 21 August 2017; Received in revised form 24 March 2018; Accepted 27 September 2018
Available online 03 October 2018
0149-1970/

Nomenclature

A	Area, m^2
De	Equivalent diameter (m)
f	Friction coefficient
H	Specific enthalpy ($J{\cdot}kg^{-1}$)
k	Thermal conductivity ($W{\cdot}m^{-1}{\cdot}^oC^{-1}$)
k_a	Coefficient of acceleration pressure drop
k_c	Coefficient of local resistance
L	Length (m)
l_i	Length of control volume i (m)
m_i	Mass of control volume i (kg)
P	Pressure (Pa)
q	Heat flux ($J{\cdot}s^{-1}$)
t	Time (s)
T	Temperature (K)
U	Wetting perimeter (m)
W	Mass flow rate, ($kg{\cdot}s^{-1}$)
z	Axial coordination (m)

Greek symbols

ρ	Density ($kg{\cdot}m^{-3}$)
ϕ	Heat flux ($J{\cdot}s^{-1}$)
Δp	Variation of fluid pressure (Pa)

subscripts

i	Control volume i
in	Inlet
N	Control volume number
out	Outlet

usually attached to the inner thermal baffle to create a gap filled with motionless sodium, which contributes to weakening the thermal stress of the baffles. The main vessel is surrounded by the guard vessel with insulting layer attached outside, and the gap between main vessel and guard vessel is filled with inert argon. The guard vessel provides a double guarantee to prevent the leakage of sodium. The Reactor Air Cooling System (RACS) in the pit of the reactor and the concrete in its outer side are also included in RVCS. The air flows upwards from the bottom of the reactor pit and removes the heat of the system. In the accident of black out, the natural convection of the air as well as the radiation between the concrete and the insulting layer also contribute to the decay heat removal.

As shown in Fig. 3, the main vessel and the thermal baffles have created two annuluses, i.e. outer annulus and inner annulus, to allow the cold sodium passing by. Under normal operating condition, cold sodium pumped from the cold pool flows upwards through the outer annulus and finally returns to the cold pool by flowing downwards in the inner annulus. The cold sodium in the annulus absorbs heat from the hot pool along its flow path. On one hand, the fluids take the heat into the cold pool, and on the other hand the main vessel is protected from being heated up by the hot pool. When accidents occur, the pump driving force disappears and the fluid in RVCS may flow reversely under the natural circulation condition. The reverse fluids would flow into the grid plate, one of whose outlets is connected to the inlet of RVCS originally under normal operating condition, and finally the reverse fluids would flow into the core under natural circulation.

Generally, the upward fluid in the outer annulus flows into the inner annulus in two ways as shown in Fig. 4. Many SFRs adopted the way of Path 1, i.e. climbing over the wall, including almost all the SFRs in Indian such as PHENIX (IAEA-TECDOC, 2013) and Demonstration Fast Breeder Reactor (DFBR) (Vivek et al., 2013). However, others such as MONJU (Ohira et al., 2013) and CEFR employed the way of the path 2, i.e. flowing through the hole. Both the two ways have their advantages and disadvantages. For path 1, when the flow is strong, the fluid in the upward flow climbs over the wall and then dumps into the inner annulus, acting as a waterfall. It's a very strong stress shock on the thermal baffle. While for the fluid flow in path 2, it can avoid the waterfall by flowing through the hole. However, the existence of the hole may affect the structural integrity of the material which will be a threaten to the safety, stability and ability to withstand stress of the thermal baffles.

Many countries have developed computer codes to calculate thermo-hydraulics for SFR, including the RUBIN and GRIF in Russia, the OASIS and TRIO-U in France (Tenchine et al., 2012), the SAS4A in America (Cahalan and Wei, 1990; Cahalan et al., 1994; Fanning, 2012) and so on. Generally, those codes aim at the whole system analysis, but little attention has been given to the study on transient characteristics of RVCS. In present work, the performed study on RVCS is mainly confined to the CFD simulation. Vivek v et al. proposed a CFD based approach to study the effect of ovality and the uniformity of sodium flow in the main vessel cooling system for pool-type sodium-cooled fast reactors (Vivek et al., 2013). Another CFD simulation proposed by T.C. Hung et al. also concluded that RACS is effective in removing decay heat after shut down (Hung et al., 2011). What's more, an experimental study on DFBR has been conducted and temperature distributions in the main vessel cooling system are carried out (Kamzaki et al., 1995).

In fact, it's difficult for CFD to simulate the whole system under a reasonable run-time (Feng et al., 2017). It's very hard to evaluate the impact that the RVCS plays on the transient characteristics of the whole system by CFD method. Thus, the one-dimensional approach is effective to simulate the thermal-hydraulic characteristics of RVCS as well as the thermal-hydraulic response to the transient process of the primary loop in SFRs.

In China, the research of the thermo-hydraulics for SFR is very few. Most studies are focus on the Pressurized Water Reactor (PWR). Feng T et al. proposed an innovative Direct Residual Heat Removal System (DRHRS) to study the capability of removing the residual heat of CPR1000 (Feng et al., 2016). Xi'an Jiaotong University has developed a program MIDAC to analyze the processes of in-vessel severe accident in CPR1000(Wang et al., 2014a,b). Cui S et al. also carried out some numerical research on the thermal-hydraulic characteristics of the Chinese Fusion Engineering Test Reactor (CFETR) (Cui et al., 2017). To support the development of sodium-cooled fast reactor in China, this paper has developed a home-made one-dimensional (1-D) code named Reactor Vessel Cooling system Analysis Code for Sodium-cooled fast reactor (VECAS) to evaluate the thermal-hydraulic characteristics for SFR. Not only can this code simulate the thermal-hydraulic characteristics of RVCS itself but also it can be coupled with a 1-D system analysis code THACS (Ma et al., 2015; Yue et al., 2015) with quick computing speed. This paper has performed the calculation of CEFR and sensitivity analysis of the main parameters in RVCS with the coupled code. This code has the ability of the parametric sensitivity analysis, optimal design of system, and evaluation of decay heat removal capacity.

2. Models and methods

The control volume of the main components in RVCS is shown in Fig. 5. The components in the model contain the fluid domain, the solid domain and the gas domain. The fluid domain consists of the upward fluid and the downward fluid. The main vessel, the thermal baffles in its inner side and the guard vessel, the insulating layer, the concrete in its outer side are included in the solid domain. The argon gap and the air cooling system in the pit of the reactor as the gas domain are also taken into consideration.

For the fluids in the annuluses, the convection heat transfer with the

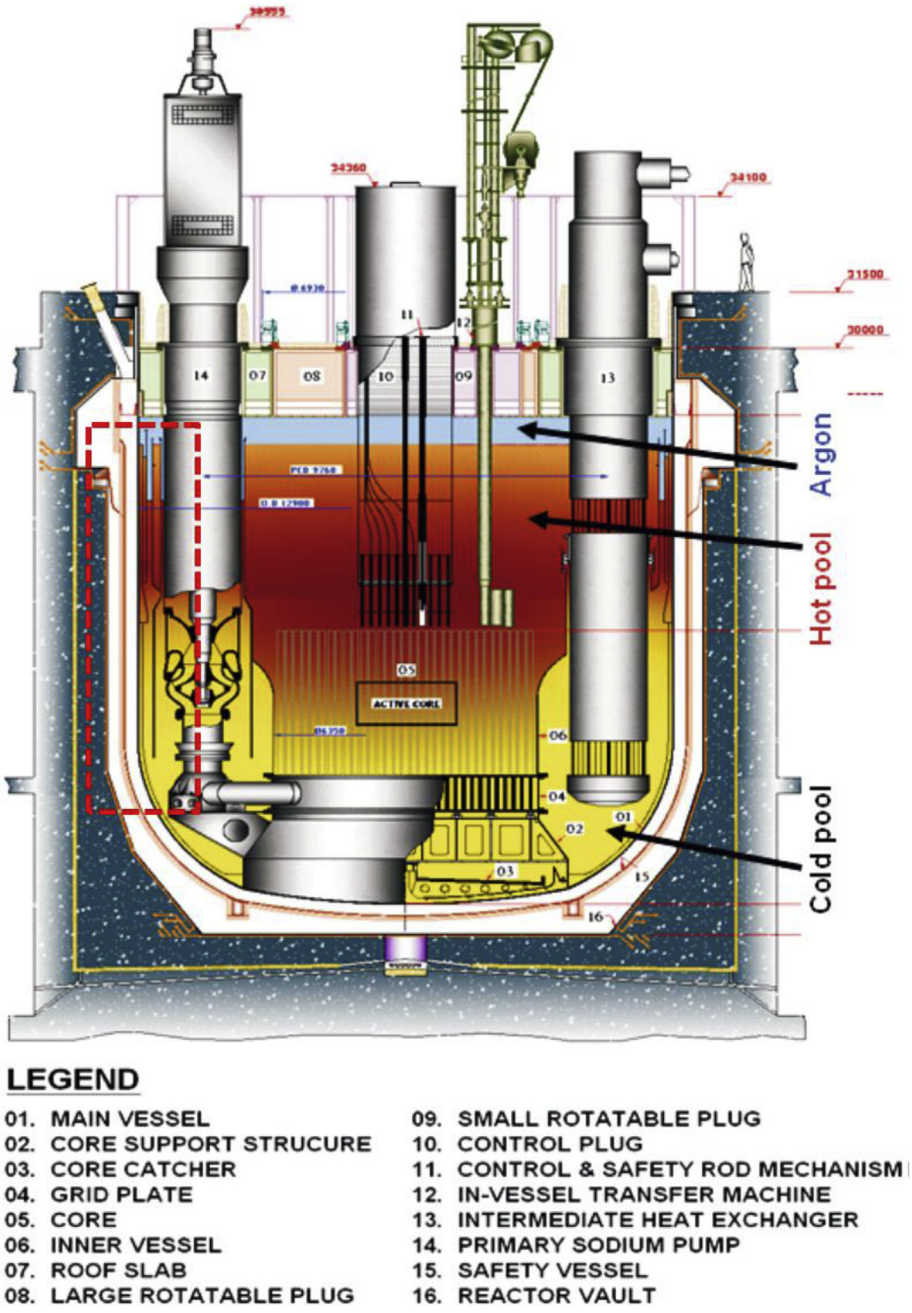

Fig. 1. Reactor structure of PFBR (Velusamy et al., 2010).

walls in its both sides is taken into consideration. The axial heat conduction is small enough to be ignored for the flowing sodium. Sodium is considered incompressible and the density of sodium is only a function of temperature. According to the structure difference, the module is divided into single channel region and dual channel region as shown in Fig. 6. In the dual channel region, the upward and downward fluids are both included in the fluid domain.

2.1. Models for the fluid in the single channel region

Based on above assumptions and the region dividing, for the fluid in the single channel region, we can get the governing equations from the simplified basic equations of mass, momentum and energy as:

$$\frac{\partial}{\partial z}\left(\frac{W}{A}\right) = 0 \tag{1}$$

$$\frac{L}{A}\frac{dW}{dt} = P_{in} - P_{out} - \Delta P \tag{2}$$

$$A\rho\frac{\partial H}{\partial t} + W\frac{\partial H}{\partial z} = \frac{qU}{A} \tag{3}$$

As shown in Fig. 7, the staggered mesh is adopted to the equation discretization. The parameters of enthalpy, pressure are located in the main control volume, while mass flow in the momentum control volume. According to Eq. (1)-Eq. (3), the equations can be discretized as:

$$W_i = W_{i-1} \tag{4}$$

$$\frac{dW_i}{dt} = \frac{P_{\text{in}} - P_{\text{out}} - \sum_{i=1}^{N}\Delta P_i}{\sum_{i=1}^{N}\frac{l_i}{A_i}} \tag{5}$$

$$\frac{dH_i}{dt} = \frac{W_i(H_{i-1} - H_i) + q_i U_i l_i}{A_i \rho_i l_i} \tag{6}$$

Where subscript i is the control volume numbers, and $\sum_{i=1}^{N} \Delta P_i$ is the pressure drop consisting of the friction, acceleration, gravity and local resistance pressure drop as the following equation (G.H.Su et al., 2013):

$$\Delta P_i = \frac{f_i l_i W_i |W_i|}{2D_{e,i}\rho_i A_i^2} + \rho_i g l_i + \frac{k_{a,i} W_i |W_i|}{2\rho_i A_i^2} + \frac{k_{c,i} W_i |W_i|}{2\rho_i A_i^2} \tag{7}$$

2.2. Models for the fluid in the dual channel region

According to the introduction, we know that the upward fluid in the outer annulus flows into the inner annulus in two ways. The mathematical physical model of Path 1 is relatively simpler than that of path 2. When the fluid flows in path1, it's only a matter of boundary transfer. The fluid will flow directly to the inlet of the inner annulus with its original mass flow rate and temperature in the outlet of the outer annulus. It doesn't matter the height difference of liquid levels, which will make the problem easier. This part will focus on the models for path 2.

In RVCS, the upward and downward fluids share the same argon space with the same pressure. The compressible argon gas with constant pressure makes it possible for the liquid level to change in a transient process. The height difference of liquid levels in the two channels determines the flow rate and its direction. Under normal operating condition, the pump drives the fluid to flow upwards in the outer annulus and flow into the inner annulus through the hole. The liquid level in the outer annulus is higher than that in the inner annulus. When the pump driving force disappears under accident conditions, the fluid expands with the heat from hot pool. The liquid level in the outer annulus becomes lower than that in the inner annulus, and the density difference of fluid may drive a reverse flow.

Fig. 8 shows the control volumes of the fluids in dual channel region. The mass change rate is determined by the mass flow rate flowing in and out of the control volume, while the inlet and outlet pressure and its pressure drop determine the mass flow rate change rate in the annulus except the control volume at the hole. The mass continuity equation and the momentum conservation equation are shown below:

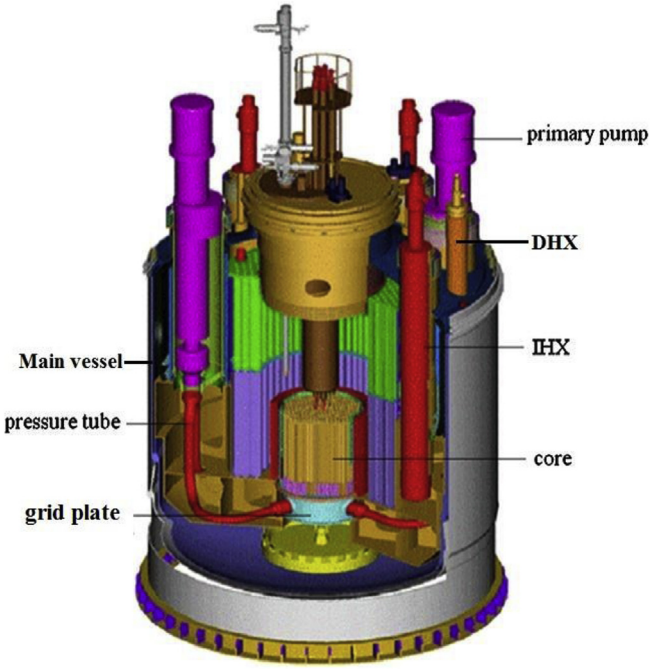

Fig. 2. Reactor structure of CEFR (Cui et al., 2013).

$$\frac{dm_i}{dt} = W_{i,in} - W_{i,out} \tag{8}$$

$$\frac{L_i}{A_i}\frac{dW_i}{dt} = P_{i,in} - P_{i,out} - \Delta P_i \tag{9}$$

With the known mass in each control volume, we can get the actual height of control volume i by

$$H_{cv,i} = \frac{m_i}{\rho_i A_i} \tag{10}$$

And the actual height of the coolant level can be gained by summing up all the actual height of the control volume.

$$H = \sum_{i=2}^{n+1} H_{cv,i} \tag{11}$$

The coolant height over the hole h is the difference of H and the already known length L of the liquid below the hole.

$$h = H - L \tag{12}$$

We assume that the fluid over the hole is almost static and the pressure at the hole is constant argon pressure adding up the gravity pressure drop.

$$P_{1,\text{out}} = P_0 + \rho_1 g h_1 \tag{13}$$

$$P_{2,\text{in}} = P_0 + \rho_2 g h_2 \tag{14}$$

Where, the subscripts 1 and 2 represent the fluids in the outer and inner annulus respectively.

Thus, the local resistance pressure drop at the hole is given by

$$\Delta p_c = P_{1,\text{out}} - P_{2,\text{in}} \tag{15}$$

The mass flow rate at the hole is determined by

$$\Delta p_c = \frac{f_c W_c |W_c|}{2\rho_1 A_c^2} \tag{16}$$

And the mass flow rate of the upward and downward fluid when $i = N + 2$ equals to W_c, that is

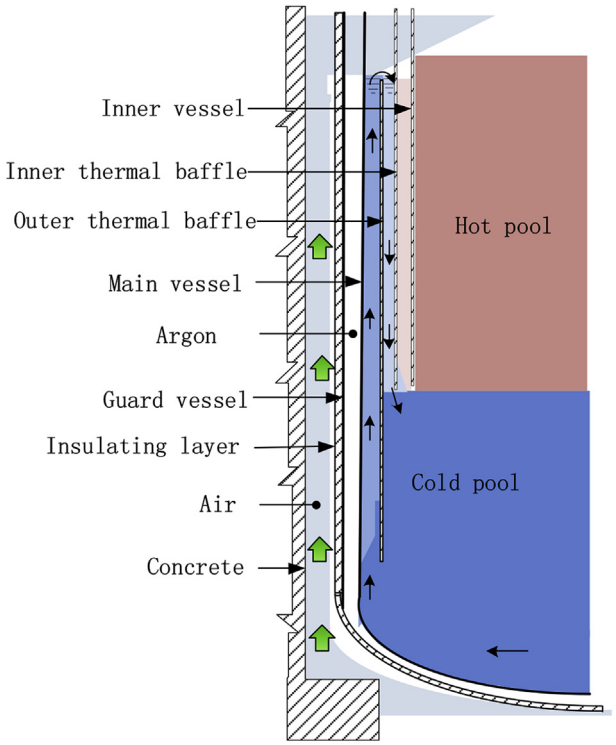

Fig. 3. The simplified schematic of RVCS.

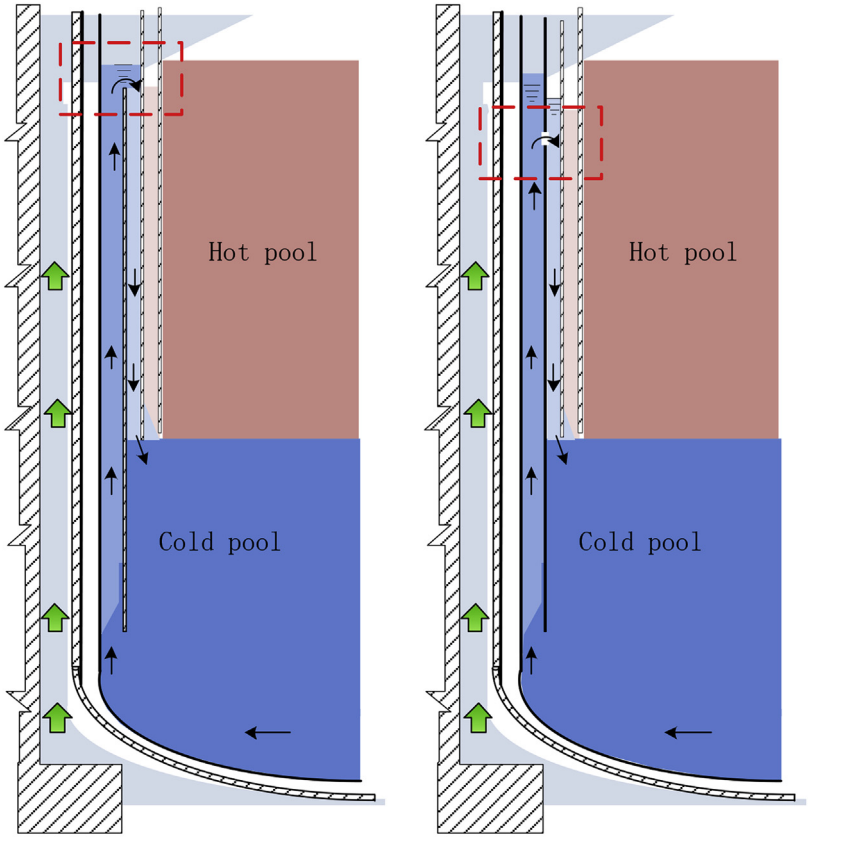

Fig. 4. Simplified diagram of fluid flow mode.

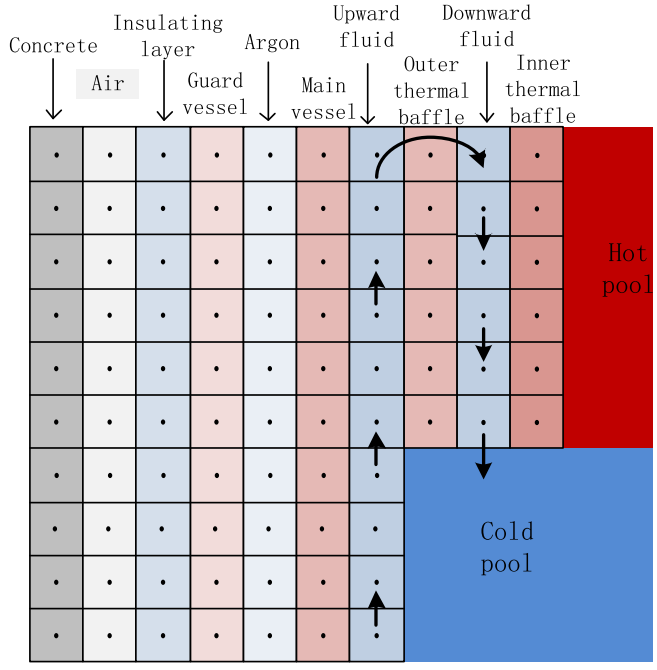

Fig. 5. Control volumes of RVCS.

$$W_c = W_{1,out} = W_{2,in} \tag{17}$$

Where, the subscript c represents the fluid at the hole in eq. (15)-eq. (17).

Different from the energy conservation equation in single channel region, the energy conservation equation in dual channel region doesn't ignore the energy change resulting from the change of the mass in the control volume. The energy conservation equation can be written as follows:

$$A_i \rho_i l_i \frac{\partial H_i}{\partial t} + W_i l_i \frac{\partial H_i}{\partial z} + H_i \frac{\partial m_i}{\partial t} = \Phi \tag{18}$$

2.3. Models for the solid walls and gases

For other solid walls and gases, such as the inner thermal baffle, outer thermal baffle, the main vessel, the argon gas gap, the guard vessel, insulting layer, the air cooling system in the pit of the reactor and the concrete in its outer side, consider the radiation heat exchange, convection heat transfer and heat conduction in accordance with actual conditions.

Taking the main vessel for example, the radiation heat exchange with the guard vessel, convection heat transfer with the upward fluid and the heat conduction itself are taken into consideration.

Ignoring axial heat conduction, the governing equation of the wall or gas k in one-dimensional model is shown below:

$$A_k \rho_k c_k \frac{dT_k}{dt} = \sum_j \phi_{jk} \tag{19}$$

$$\phi_{jk} = k_{jk} U_{jk} (T_j - T_k) \tag{20}$$

2.4. Numerical method

All of the models developed above can be converted into the style of

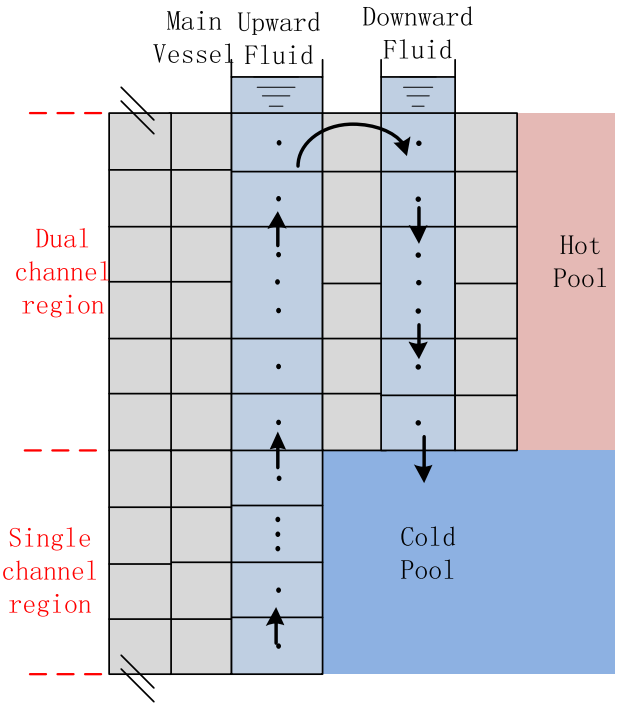

Fig. 6. The schematic diagram of the dividing region.

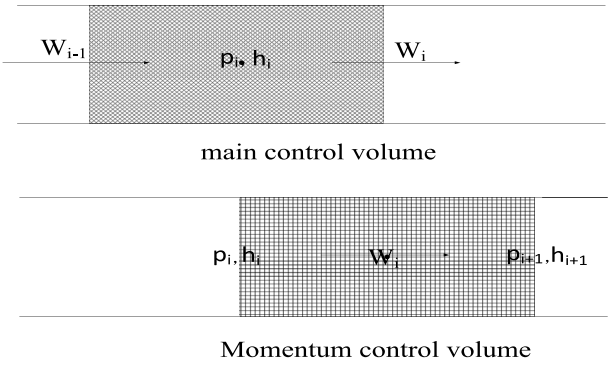

Fig. 7. Mesh of the control volume.

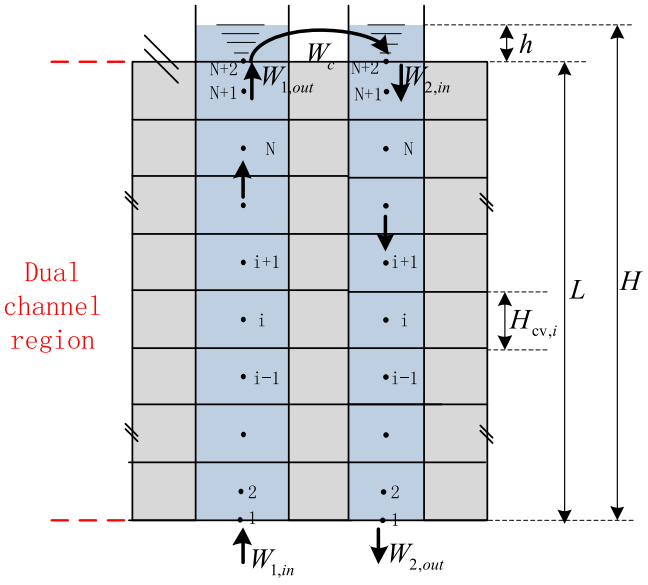

Fig. 8. The control volumes of dual channel region.

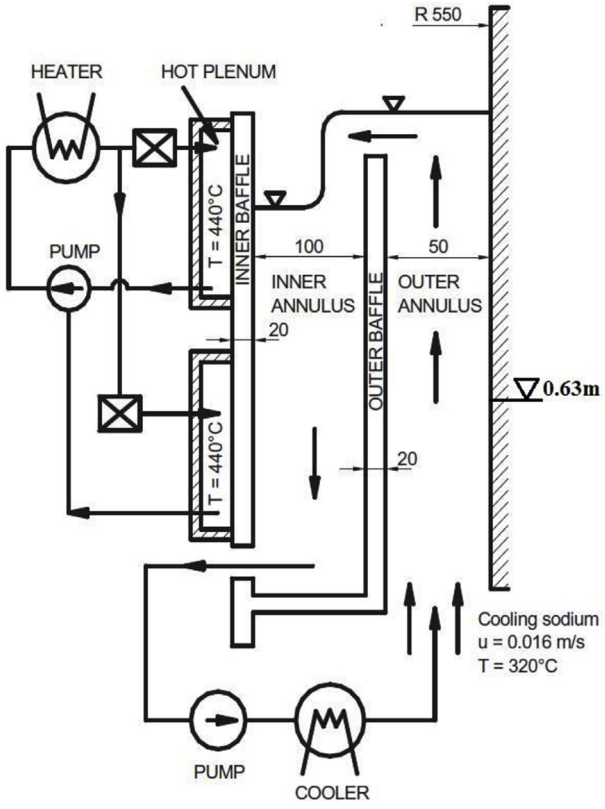

Fig. 9. Experimental apparatus of DFBR (Vivek et al., 2013).

the ordinary differential equations, which will lead to a large initial value problem of the parameters:

$$\begin{cases} \frac{d\vec{y}}{dt} = f(t, y, y') \\ \vec{y}(0) = \vec{y_0} \end{cases} \tag{21}$$

VECAS has adopted Gear method (Gear, 1971) to solve these stiff equations, which has obtained good results with high solving accuracy and fast computing speed.

3. Validation of VECAS

The code is validated against an experimental study on the main vessel cooling circuit of Japanese reactor, i.e. the Demonstration Fast Breeder Reactor (DFBR). Kamzaki et al. carried out the experiment and reported the experimental data of the temperature distributions in RVCS. The experimental apparatus of DFBR is shown in Fig. 9. The main vessel is simulated by a cylindrical vessel with inner diameter of 1.1 m and height of 2 m. The outer and inner thermal baffles are simulated by two concentric baffles with 20 mm in thickness. The outer annulus and inner annulus are formed for the sodium to pass through with width of 50 mm and 100 mm respectively. The inner baffle is close to the hot pool filled with the hot sodium at 440 °C. Pump drives the coolant in the main vessel circuit. The cooling sodium flows upwards through the outer annulus and finally returns to the cold pool by flowing downwards in the inner annulus. The mass flow rate of the coolant is 2.27 kg s^{-1} with inlet temperature of 320 °C.

The validation of VECAS is performed based on the real experimental parameters. Physical model of the real geometric design is shown in Fig. 10. The temperature distributions in the radial direction at the height of 0.63 m are compared with the experimental data. As shown in Fig. 11, the calculation results match very well with the experimental data, and the maximum of relative error is 1.1%. The relative error is calculated by

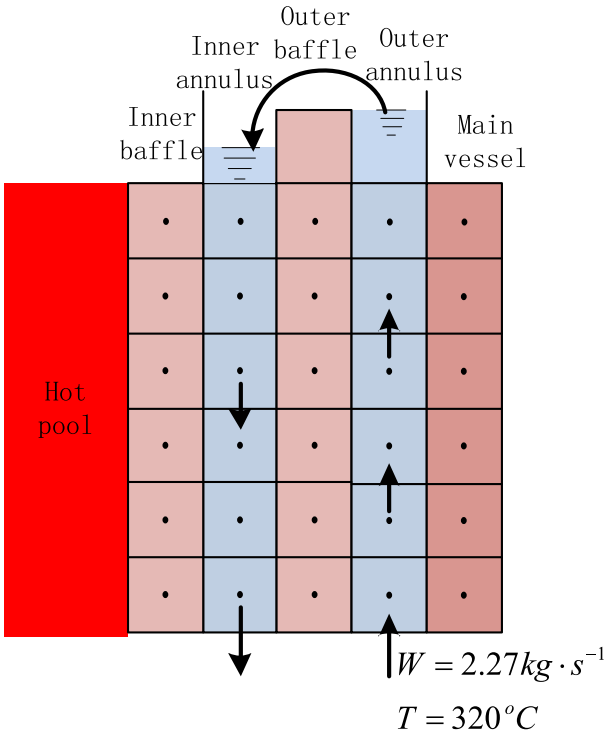

Fig. 10. Physical modeling.

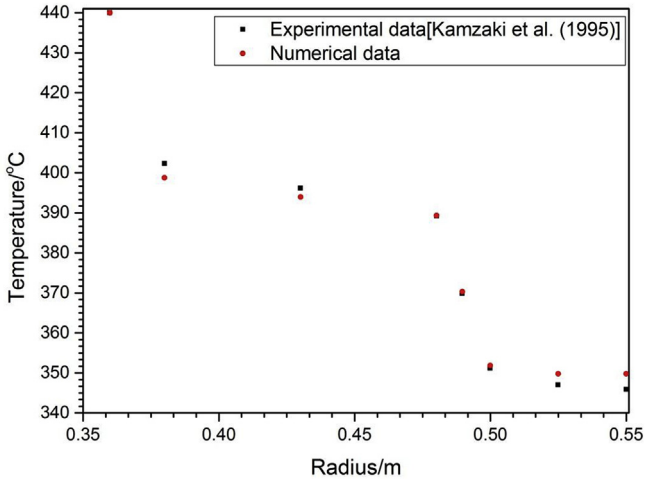

Fig. 11. Comparison of temperatures at 0.63 m elevation.

$$\delta = \frac{|T_e - T_n|}{T_e} \times 100\% \quad (22)$$

Where, T_e is the temperature of experimental data, and T_n is the temperature of numerical data.

4. Analyses of RVCS characteristic for CEFR

4.1. The steady-state analysis

The steady analysis of RVCS is performed based on the operation parameters of CEFR. Fig. 5 shows the control volumes of the main components in RVCS. The thickness of main vessel and guard vessel are 25 mm and the width of the outer annulus and inner annulus are 45 mm. The temperatures of the cold and hot pool are 360 °C and 516 °C, respectively. The flow mass of the fluid is 40 kg s^{-1} (Qiao et al., 2006). Some main parameters of RVCS is listed in Table 1.

Fig. 12 is the temperature of the upward and downward fluid in the annulus. As can be seen, the temperature of the downward fluid is always higher than that of the upward fluid in the same axial position. The fluid brings the heat from the hot pool to the cold pool continually with its temperature increasing along its flowing direction.

As shown in Fig. 13, the temperature of the main vessel is close to the temperature of the upward fluid and much higher than that of the downward fluid. Compared with the hot pool temperature of 516 °C, the main vessel is cooled effectively. The maximum temperature of the main vessel is about 406 °C which occurs at the top of the main vessel. The results indicate that the temperature of main vessel is within the temperature limit of stainless steel and RVCS is able to cool the main vessel and enhance its structural integrity effectively.

4.2. The transient analysis

Transient Thermal-Hydraulic Analysis Code for Sodium-cooled fast reactors (THACS) is a 1-D system analysis code developed by Xi'an Jiaotong University. The code employed the object-oriented modular modeling method with the property of good portability. Thus, THACS can simulate many kinds of SFRs for thermal-hydraulic analysis. In this part, VECAS is coupled with THACS to simulate the transient characteristics of RVCS based on the station blackout (SBO) accident of CEFR. In the transient analysis, the time step is changeable base on the method of Gear algorithm, and the change range of the time step is usually between $10^{-3}$and 10^{-5}.

CEFR is the first fast reactor in China. It's a pool-type sodium-cooled fast reactor operating at a thermal power of 65 MW and electrical power of 25 MW (Qiao et al., 2006). The coolant is pumped from the cold pool to flow into the grid plate through the pressure tube. Then the coolant at 360 °C is discharged into the core inlet, and the core outlet temperature will be 530 °C after heated in the core. The average temperature of the hot pool is 516 °C, from which the sodium flows into four intermediate heat exchangers and then goes back to the cold pool at the temperature of 353 °C. The cold sodium mixes with other inlet sodium in the cold pool, making the average temperature in the cold pool 360 °C. The simplified schematic diagram of CEFR is shown in Fig. 14. The components of the system simulated in the transient analysis are listed in Table 2.

In the SBO accident, core power decreases from 0 s, the pump speed reduced to 0 rpm in 40 s, and the secondary mass flow rate of IHX reduced to 0 kg s^{-1} in 20 s. The sequence of SBO is shown in Table 3. The normalized variations of core power, pump speed and secondary mass flow rate in IHX are shown in Fig. 15 (Cui et al., 2013).

Fig. 16 shows the normalized mass flow rate in RVCS. As the pump speed drops, the pump driving force disappears gradually. It can be seen that the mass flow rate decreases with the pump speed and becomes negative at 26s. Thus, VECAS has predicted a reverse flow in RVCS during the transient process.

Fig. 17 displays the variation of the height in the annuluses over time. Both the height levels of the coolant drop sharply with a decrease

Table 1
Main parameters of RVCS.

Parameters		Unite	Value
Thermal parameters	Mass flow rate	kg·s^{-1}	40
	Inlet temperature	°C	360
	Outlet temperature	°C	400
	Hot pool temperature	°C	516
	Cold pool temperature	°C	360
	Air inlet temperature	°C	50
Structure parameters	Main vessel thickness	mm	25
	Guard vessel thickness	mm	25
	Outer thermal baffle thickness	mm	10
	Outer annulus width	mm	45
	Inner annulus width	mm	45

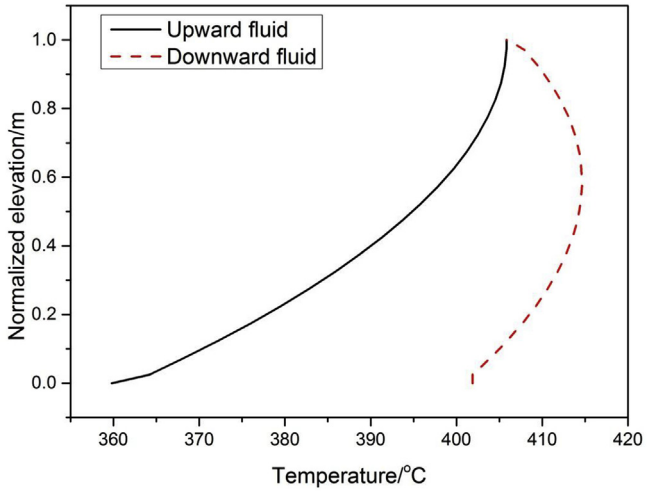

Fig. 12. Temperature of fluids.

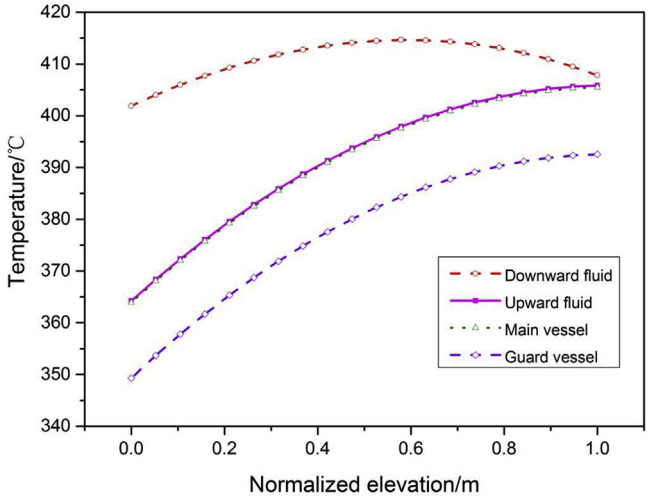

Fig. 13. Temperature of main components.

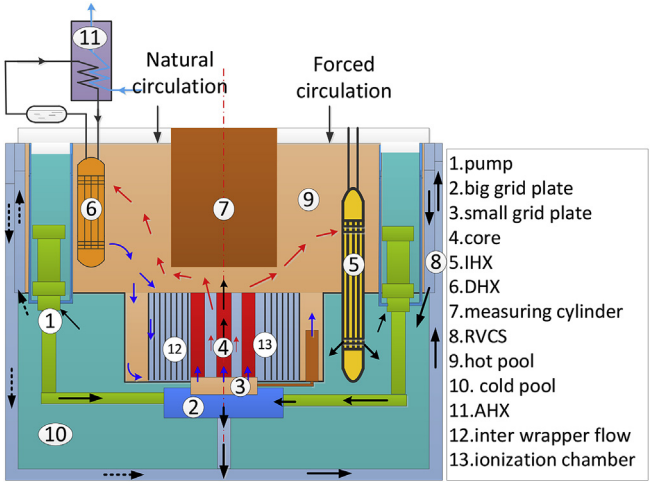

Fig. 14. The simplified schematic diagram of CEFR.

in pump speed before 3 s at the beginning and remains almost constant after 50s. Before 26s, the height of upward fluid is higher than that of downward fluid and inverse after 26s, which is closely consistent with the mass flow rate of RVCS. The results also prove that the mass flow in

Table 2
Components of the CEFR system.

Components	Number
Core	1
Inter wrapper flow	1
Cold pool	1
Hot pool	1
Pump	2
IHX	4
DHX	2
AHX	2
Grid plate	2
Ionization chamber	1
RVCS	1
PIPE	several

Table 3
Sequence of SBO.

Event	Time
SBO occurs	0.0 s
Reactor coolant pumps trip	0.0 s (power loss)
Reactor shutdown	0.0 s (control rods drop down)
RACS fan stalls	1.0 s
Coasting time of secondary pumps	20 s (isolate secondary loop)
Coasting time of primary pumps	40 s (primary pump speed reduces to 0 rpm)
Damper of AHX opens	600 s

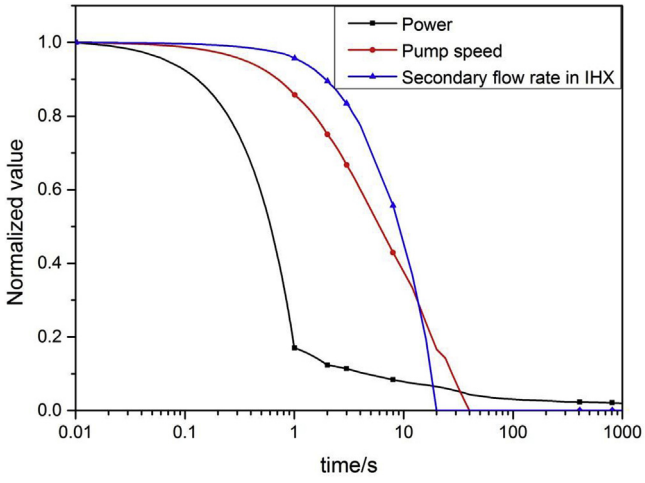

Fig. 15. The normalized variations of main parameters vs. time.

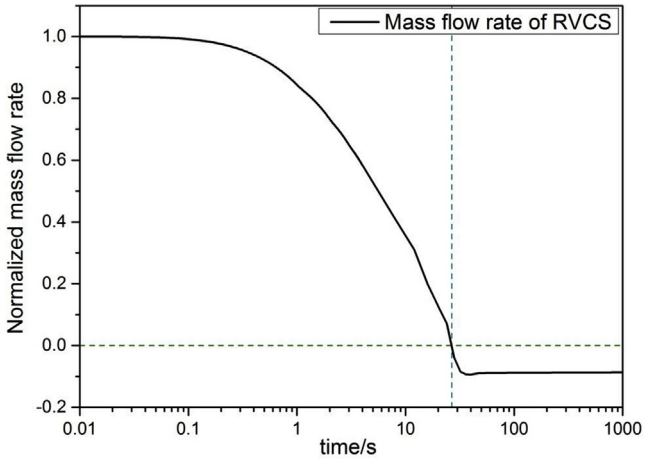

Fig. 16. The normalized mass flow rate of RVCS.

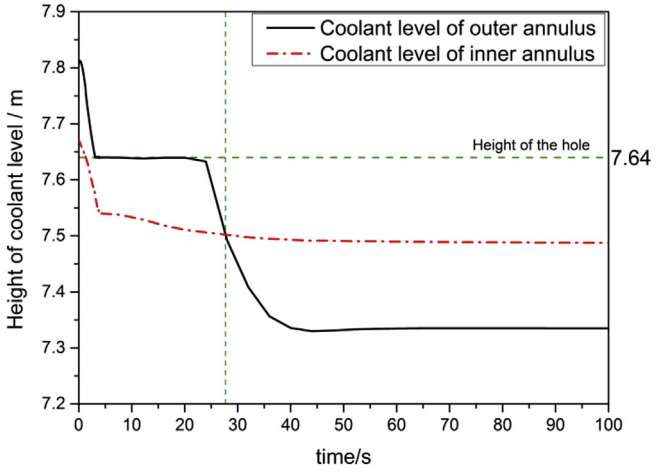

Fig. 17. The height of coolant level in the annulus.

RVCS is correlated with the height difference of liquid levels.

5. Heat removal characteristics of RVCS

In this part, the effect and heat removal characteristics of RVCS are investigated. Furthermore, sensitivity analysis is conducted to investigate the main parameter, which has great effect on core cooling. The analyses are based on the same sequence of the SBO accident of CEFR as described in section 4.2.

5.1. Research on the effect of RVCS

RVCS is designed to cool the main vessel and enhance its structural integrity on original purpose. However, only a few researches on the effects for the core cooling were published. Thus, two transient cases are developed to study the heat removal capability of RVCS. The only difference of the transient cases is whether the RVCS is simulated or not.

Fig. 18 and Fig. 19 show the comparisons of the core outlet temperature and core mass flow rate in the two transient cases. As shown in the figures, the variation trends of the core outlet temperature and mass flow rate are similar. Before the first temperature peak at about 90 s, the core outlet temperatures of the two cases are almost the same. During the establishment of the natural circulation, the core outlet temperature of the system without RVCS is higher than that with RVCS. Temperature difference at the two peaks is about 2 °C and the difference reaches 5 °C at 2600 s. It should be noticed that in the simulation both the two AHX are put into use and the main way of heat removal is by DHX-AHX, under which condition RVCS is an auxiliary cooling system. Therefore, the temperature difference is only 5 °C, which still illustrates that RVCS indeed contributes to the core cooling. As shown in Fig. 19, after the stop of the pump, the natural circulation flow in the core of the system with RVCS is higher than that without RVCS.

The comparison of heat removal rate is shown in Fig. 20. The whole decay heat removal rate means the proportion of the core decay heat that the heat removed out of the system accounts for. Considering that the secondary side of IHX is isolated in 20s, the whole decay heat removal in Fig. 20 mainly contains the decay heat removed by DHX and RVCS (if any). As shown in Fig. 20, the trends of whole decay heat removal rate in the two cases are similar, and the decay heat rate with RVCS in CEFR is always higher than that without RVCS. Obviously, the difference comes from the decay heat removed by RVCS. At 2800s, the whole decay heat removal with RVCS in CEFR reaches 106.7%, exceeding the core decay heat, while that without RVCS is only 91.8%. It should be noticed that the decay heat rate appeared a sudden increase from about 600s to 1000s, resulting from the opening of AHX damper at 600s.

The variation of heat removal by RVCS and heat removal rate is shown in Fig. 21. The stalling of the fan installed in RACS results in the heat removal by RVCS dropping sharply at the beginning of SBO. Then the heat removal by RVCS increases. At the early stage of SBO, the temperature in the hot pool changes slowly for the big heat capacity of sodium and thermal stratification in the hot pool. While the temperature in the cold pool rises rapidly due to the high-temperature sodium from the IHX. Thus, the temperature difference between the inner reactor vessel and the outside becomes bigger, which results in the increase of the heat removal by RVCS. As the system levels off at the late stage of SBO, the heat removal by RVCS and the heat removal rate remain almost unchanged at the value about 83.9 kW and 12%, respectively. The heat removal rate by RVCS means the proportion of the core decay heat that the decay heat removal by RVCS accounts for.

Comparisons of two transient cases present that the reverse fluid of RVCS contributes to the core cooling and decay heat can be removed efficiently by RVCS.

5.2. Sensitivity analysis

Simulation results of two developed transient cases have presented that reverse fluid contributes to core cooling. It's significant to research the influence extent of the reverse mass flow rate on the heat decay capacity and the determinant of the mass flow rate. Thus, this paper has performed sensitivity analysis about five different sizes of the reverse hole area in RVCS. In the analysis, we assume that the reverse hole area is 1A in the reference case, and the reverse hole areas are 0.25A, 0.5A, 2A and 4A in other cases, respectively.

As shown in Fig. 22, the reverse mass flow rate of RVCS increases with the increase of the reverse hole area. As shown in Fig. 23, after the first temperature peak at about 80s, differences occur among the five core outlet temperatures, and the core outlet temperature of bigger hole area is lower than that of smaller hole area. Thus, the core outlet temperature rises when the reverse hole area decreases. Table 4 displays main parameter comparisons at 3000 s. At 3000 s, temperature difference between the 0.25A and 4A reaches 7.50 °C and RVCS reverse mass flow rate difference is 3 kg s^{-1}.

The results indicate that reverse hole area is positively correlated to the reverse mass flow rate of RVCS. And the results of sensitivity analysis proves that the reverse fluid of RVCS contributes to the core cooling. The bigger mass flow rate of the reverse fluid is more beneficial to the core cooling. Although bigger reverse hole area benefits the core cooling, the design of the reverse hole area should be the combination of thermal hydraulic and structure consideration.

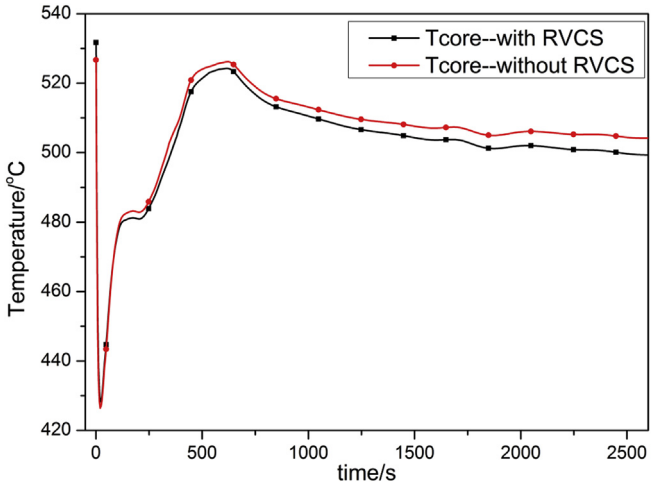

Fig. 18. The comparison of core outlet temperature.

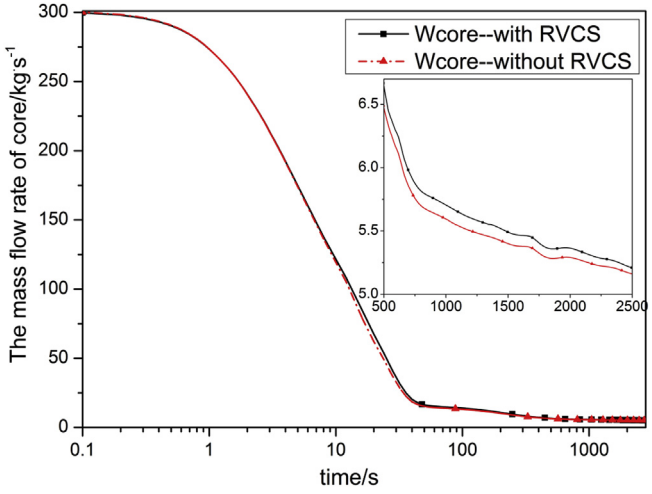

Fig. 19. The comparison of core mass flow rate.

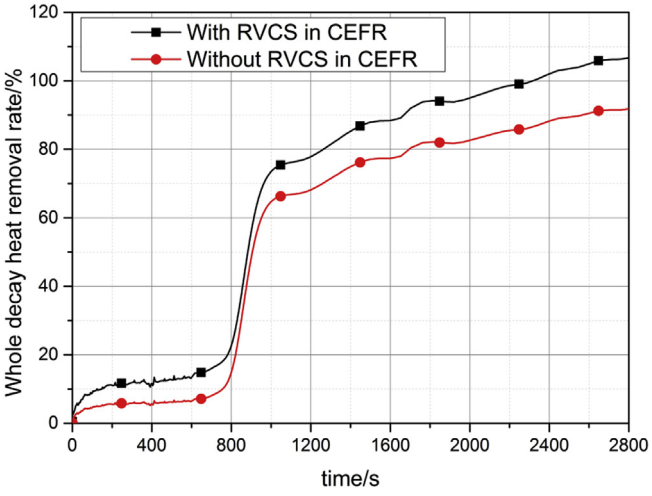

Fig. 20. The comparison of heat removal rate.

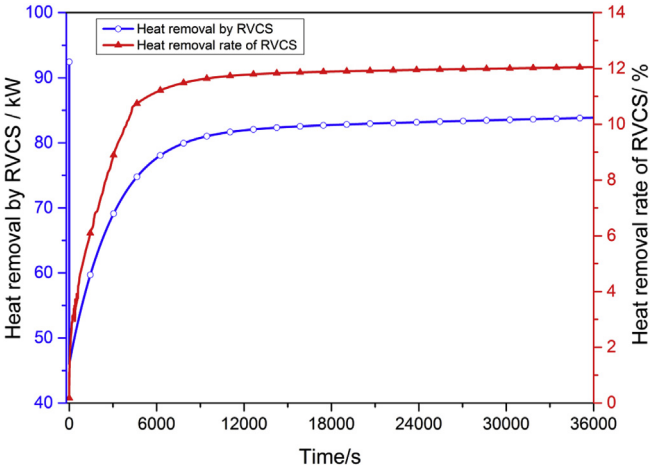

Fig. 21. Variation of heat removal by RVCS and heat removal rate.

6. Conclusion

In this paper, a one-dimensional code VECAS has been developed to simulate the thermal-hydraulic characteristics of RVCS for SFRs. The code has been validated against the main vessel cooling circuit of DFBR, and the simulation results are in good agreement with the experimental data. The steady analysis results of CEFR agree well with the design value and indicate that RVCS is able to cool the main vessel and enhance its structural integrity effectively.

VECAS is coupled with THACS to calculate the transient characteristics of RVCS in CEFR. The simulation has predicted a reverse flow in RVCS in the whole transient process. Sensitivity analysis of the main parameters of RVCS has also been performed based on the SBO of CEFR. The results imply that RVCS contributes to the core cooling and decay heat can be removed efficiently by RVCS.

Based on the analytical investigations, VECAS has the ability to evaluate the thermal-hydraulic characteristics and the decay heat removal capacity of RVCS. Moreover, the code can be coupled with system analysis code easily with a quick computing speed. VECAS could provide references and technical supports for the design and optimization of the pool-type sodium-cooled fast reactor, especially for the development of SFRs in China.

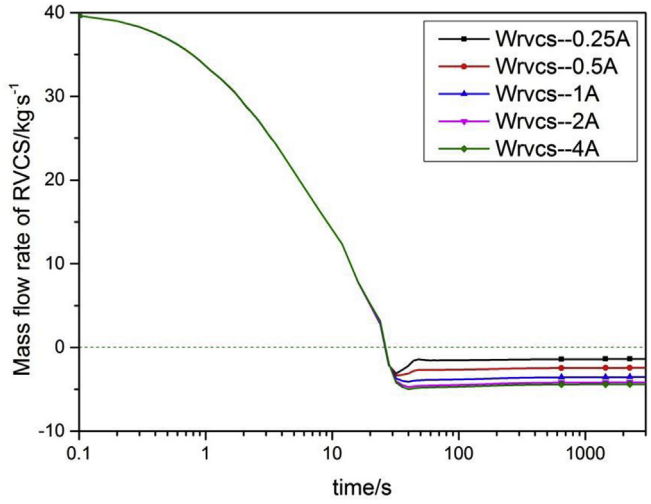

Fig. 22. The comparison of RVCS mass flow rate.

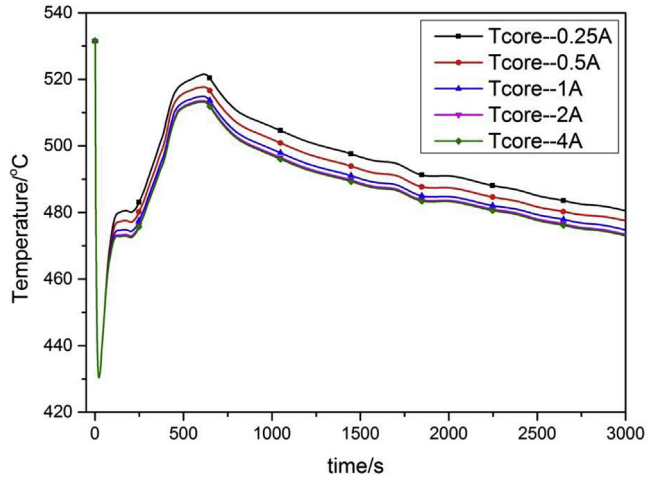

Fig. 23. The comparison of core outlet temperature.

Table 4
Main parameter comparisons at 3000 s.

Parameters Value	0.25A	0.5A	1A	2A	4A
RVCS reverse mass flow rate ($kg{\cdot}s^{-1}$)	−1.38	−2.43	−3.53	−4.16	−4.38
Core mass flow rate($kg{\cdot}s^{-1}$)	5.40	5.52	5.62	5.65	5.66
Core outlet temperature (°C)	478.37	475.33	472.46	471.48	470.81

Acknowledgments

1 The authors would like to thank the support from National Natural Science Foundation of China (Grant No. 11605131) and National Natural Science Foundation of China (Grant No. 11705139).

References

Cahalan, J.E., Wei, T.Y.C., 1990. Modeling Developments for the SAS4A and SASSYS Computer Codes. Argonne National Lab., IL (USA).

Cahalan, J.E., Tentner, A.M., Morris, E.E., 1994. Advanced LMR Safety Analysis Capabilities in the SASSYS-1 and SAS4A Computer Codes. Argonne National Lab.

Chen, J., Zhang, D., Song, P., et al., 2018. CFD investigation on thermal-hydraulic behaviors of a wire-wrapped fuel subassembly for sodium-cooled fast reactor. Ann. Nucl. Energy 113, 256–269.

Chetal, S.C., Balasubramaniyan, V., Chellapandi, P., et al., 2006. The design of the prototype fast breeder reactor. Nucl. Eng. Des. 236 (7–8), 852–860.

Cui, M., Guo, Y., Zhang, Z., 2013. Transient simulation code development of primary coolant system of Chinese Experimental Fast Reactor. Ann. Nucl. Energy 53, 158–169.

Cui, S., Zhang, D., Cheng, J., et al., 2017. Numerical research on the neutronic/thermal-hydraulic/mechanical coupling characteristics of the optimized helium cooled solid breeder blanket for CFETR. Fusion Eng. Des. 114, 141–156.

Fanning, T., 2012. The SAS4A/SASSYS-1 Safety Analysis Code system.ANL/NE-12/4. Nuclear Engineering Division, Argonne National Laboratory.

Feng, T., Wang, M., Song, P., et al., 2016. Thermal hydraulic characteristics analysis of direct residual heat removal system for China pressurized reactor. Prog. Nucl. Energy 93, 231–237.

Feng, T., Zhang, D., Song, P., et al., 2017. Numerical research on water hammer phenomenon of parallel pump-valve system by coupling FLUENT with RELAP5. Ann. Nucl. Energy 109, 318–326.

Gear, C.W., 1971. Numerical Initial Value Problems in Ordinary Differential Equations. Prentice Hall PTR.

Hung, T.C., Dhir, V.K., Chang, J.C., et al., 2011. CFD modeling and thermal-hydraulic analysis for the passive decay heat removal of a sodium-cooled fast reactor. Nucl. Eng. Des. 241 (1), 425–432.

IAEA-TECDOC, 2013. Benchmark Analyses of the Natural Circulation Test Performed during the PHENIX End-of-life Experiments: Final Report of a Co-ordinated Research Project 2008-2011. no. 1703.

Kamzaki, Y., Takeishi, M., Ueda, S., Fujimoto, T., 1995. Heat transfer studies on a reactor vessel cooling system. In: Proc. International Conference on Nuclear Engineering, Japan, pp. 35–40.

Ma, Z., Yue, N., Zheng, M., et al., 2015. Basic verification of THACS for sodium-cooled fast reactor system analysis. Ann. Nucl. Energy 76, 1–11.

Ohira, H., Xu, Y., Bieder, U., et al., 2013. Benchmark analyses of sodium natural convection in the upper plenum of the MONJU reactor vessel[C]//. In: International Conference on FAST Reactors and Related Fuel Cycles: Safe Technologies and Sustainable Scenarios.

QIAO, X., YANG, H., FENG, Y., 2006. Thermal hydro-mechanical analysis of reactor vessel cooling system under station blackout accident. Nucl. Power Eng. S1.

Su, G.H., Qiu, S., Tian, W., 2013. Thermal Hydraulic Numerical Analysis of Nuclear Power System.

Tenchine, D., Barthel, V., Bieder, U., Ducros, F., Fauchet, G., Fournier, C., Mathieu, B., Perdu, F., Quemere, P., Vandroux, S., 2012. Status of TRIO_U code for sodium cooled fast reactors. Nucl. Eng. Des. 242, 307–315.

Velusamy, K., Chellapandi, P., Chetal, S.C., et al., 2010. Overview of pool hydraulic design of Indian prototype fast breeder reactor. Sādhanā 35 (2), 97–128.

Vivek, V., Sharma, A.K., Balaji, C., 2013. A CFD based approach for thermal hydraulic design of main vessel cooling system of pool type fast reactors. Ann. Nucl. Energy 57 (57), 269–279.

Wang, J., Tian, W., Fan, Y., et al., 2014a. The development of a zirconium oxidation calculating program module for Module In-vessel Degraded Analysis Code MIDAC. Prog. Nucl. Energy 73, 162–171.

Wang, J., Tian, W., Zhang, Y., et al., 2014b. The development of module in-vessel degraded severe accident analysis code MIDAC and the relevant research for CPR1000 during the station blackout scenario. Prog. Nucl. Energy 76, 44–54.

Yue, N., Ma, Z., Cai, R., et al., 2015. Thermal-hydraulic analysis of EBR-II shutdown heat removal tests SHRT-17 and SHRT-45R. Prog. Nucl. Energy 85, 682–693.

Zhang, D., Liu, L., Liu, M., et al., 2018. Review of conceptual design and fundamental research of molten salt reactors in China. Int. J. Energy Res. 42, 1834–1848.